Estimating mixing rates from seismic images of oceanic structure

K. L. Sheen,[1] N. J. White,[1] and R. W. Hobbs[2]

Received 16 July 2009; revised 14 August 2009; accepted 26 August 2009; published 30 September 2009.

[1] An improved understanding of the spatial distribution of diapycnal mixing in the oceans is the key to elucidating how meridional overturning circulation is closed. The challenge is to develop techniques which can be used to determine the variation of diapycnal mixing as a function of space and time throughout the oceanic volume. One promising approach exploits seismic reflection imaging of thermohaline structure. We have applied spectral analysis techniques to fine-structure undulations observed on a seismic transect close to the Subantarctic Front in the South Atlantic Ocean. 91 horizontal spectra were fitted using a linear combination of a Garrett-Munk tow spectrum for internal waves and a Batchelor model for turbulence. The fit between theory and observation is excellent and enables us to deduce the spatial variability and context of diapycnal mixing rates, which range from 10^{-5} to $10^{-3.5}$m^{2}s^{-1}. **Citation:** Sheen, K. L., N. J. White, and R. W. Hobbs (2009), Estimating mixing rates from seismic images of oceanic structure, *Geophys. Res. Lett.*, *36*, L00D04, doi:10.1029/2009GL040106.

1. Introduction

[2] The vertical transfer of water properties, such as heat and salinity, across isopycnal surfaces within the deep oceans is achieved by small-scale mechanical motions. Such diapycnal mixing occurs when internal waves break and generate turbulent motions, which cause overturning of the density stratification. The spatial variability of diapycnal mixing rates has important consequences for oceanic circulation models. Recent observational studies suggest that the Southern Ocean is a key locus for a significant, and unaccounted for, proportion of the mixing budget needed to close the meridional overturning circulation [e.g., *Heywood et al.*, 2002; *Naveira Garabato et al.*, 2004].

[3] It has been demonstrated that careful processing of seismic reflection transects, which were originally designed to image the solid Earth, yield excellent images of thermohaline fine-structure down to abyssal depths [e.g., *Holbrook et al.*, 2003]. These seismic images typically have vertical and horizontal resolutions of 5–10 m and the undulatory deformation of fine-structure by the ambient internal wave field is clearly visible on length scales of 10^1–10^3 m [*Holbrook and Fer*, 2005; *Krahmann et al.*, 2008]. Acoustic energy is generated by an array of airguns which is towed behind the vessel. This energy is transmitted and reflected at boundaries within the water column where changes in acoustic impedance are produced by temperature and, to a lesser extent, salinity variations [*Ruddick et al.*, 2009]. Reflected energy is recorded by a linear array (i.e. streamer) of hydrophones, typically 3–6 km long. The resultant seismic transect is essentially a vertical slice through the oceanic volume. *Holbrook and Fer* [2005] and *Krahmann et al.* [2008] showed that spectral analysis of undulating subhorizontal reflections observed on these acoustic images can be used to estimate the energy of internal waves. We have extended and automated their approach to calculate the spatial variation of diapycnal mixing rates with depth and range along a seismic transect which runs eastwards across the Falkland Plateau at the northern boundary of the Antarctic Circumpolar Current (Figure 1).

2. Acoustic Image

[4] The seismic transect was acquired between 19th and 22nd February 1993 (Figure 2a). Standard signal processing techniques were adapted in order to optimize acoustic imaging of the water column (see *Holbrook et al.* [2003], *Ruddick et al.* [2009] and caption of Figure 2 for details). We were especially concerned with ensuring that we can accurately map oceanic fine structure. It is important that acoustic reflections are positioned correctly (i.e., migrated) and that their relative amplitudes are preserved to ensure fidelity of the thermohaline structure. Note that the configuration of the seismic experiment effectively smooths out fine structure over periods of ~30 minutes. Thus the highest frequency internal waves are slightly blurred, which, if anything, will reduce internal wave energy and mixing rate estimates.

[5] The acoustic image reveals a complex pattern of coherent reflectivity, which is essentially a map of temperature gradient throughout the water column [*Ruddick et al.*, 2009]. Previous hydrographic studies noted the presence of Antarctic Intermediate Water (AAIW) and underlying, cooler Upper Circumpolar Deep Water (UCDW) in the vicinity of our seismic transect [*Arhan et al.*, 2002a]. AAIW and UCDW waters flow northwards around the east side of the Falkland Islands into the Argentine basin, following the route of the Subantarctic Front (SAF). The SAF sits above a shoreward deepening of the AAIW/UCDW boundary and its position can be inferred from a north-south band of higher velocity surface currents at about 305° E (Figure 1). The deep-water end of the seismic transect crosses a complex region of meandering surface currents and mesoscale eddy activity. Here, a striking lens of acoustically transparent water is visible (Figure 2a). Reflections along the top of this lens are smooth and continuous. A highly disrupted zone along the western side of the lens suggests that isopycnal interleaving of water masses occurs. The seismic transect was acquired in two parts and from the spatial overlap we can

[1] Bullard Laboratories, Department of Earth Sciences, University of Cambridge, Cambridge, UK.
[2] Department of Earth Sciences, University of Durham, Durham, UK.

0094-8276/09/2009GL040106$05.00

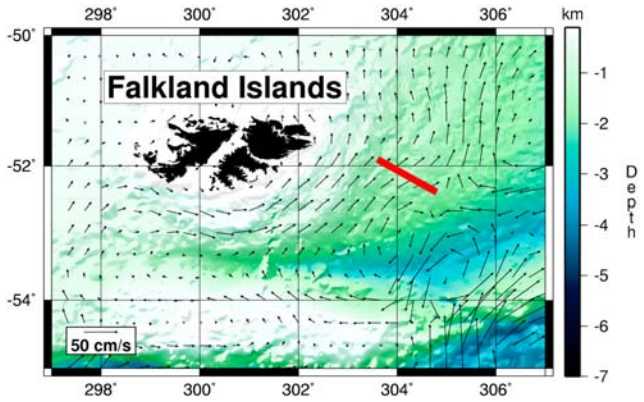

Figure 1. Bathymetry of region encompassing the Falkland Islands. Red line = seismic transect; black arrows = calculated surface geostrophic velocity vectors for 17th February 1993. Altimeter products were generated by ssalto/duacs and distributed by aviso with support from CNES (http://www.aviso.oceanobs.com/duacs/).

infer that the larger lens has travelled 10 km in 40 hours (70 mm s^{-1}). *Arhan et al.* [2002b] describe similarly homogeneous lens bodies sourced from bottom waters on the Falkland Plateau. A smaller ellipse of homogeneous water occurs at a range of ~70 km. Surface geostrophic currents show that an anti-cyclonic eddy (i.e. a cold core) is located at the end of a tongue of water, which intrudes from the east at about 53° S (Figure 1). We speculate that the two lenses are cores of cooler and well mixed UCDW. They are probably generated when circulating water masses interact with an irregular, shoaling bathymetry.

3. Spectral Analysis

[6] The cascade of energy from large-scale internal wave generating processes (e.g., winds, tides) to small-scale turbulent motion and mixing can be analyzed by calculating energy density spectra. We are principally concerned with the quasi-horizontal variation of wave energy which can be measured from vertical displacements of isopycnal surfaces. In the open ocean, towed displacement spectra (denoted by ϕ_ζ) exhibit remarkably uniform behavior which can be divided into two distinct regimes. At low wavenumbers associated with internal waves, spectra are consistent with the *Garrett and Munk* [1975] model (GM75) which obeys a power law relationship with an exponent of −2.5. At higher wavenumbers, turbulence starts to dominate and spectral slopes whiten, exhibiting Kolmogorov-like behavior (i.e.,

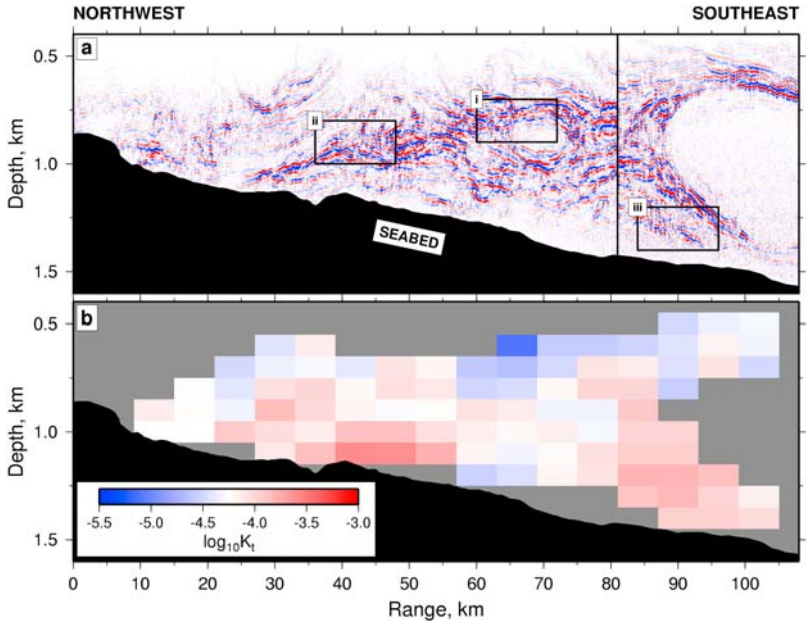

Figure 2. (a) Seismic transect which crosses Sub-Antarctic Front on the Falkland Plateau (Figure 1). Data were acquired by WesternGECO Ltd in February 1993 using the *Akademik Shatsky* which travelled at ~2 m s^{-1}. An array of bolt airguns with a total volume of 7288 cubic inches and a frequency range of 10–100 Hz was towed at 7.5 m and fired every 40 m distance. Reflected acoustic waves were recorded on a 4.8 km long streamer, which had 240 hydrophones spaced every 20 m. Streamer was towed behind vessel in a water depth of 10 m. Data sample rate was 2 ms and the first second was not recorded. Transect was acquired in two parts, delineated by a solid vertical line. Standard signal processing was carried out. A low-cut filter (≥10 Hz with a roll-off of 24 dB/octave) was applied and direct arrival was removed using a median filter. Stacking velocities were carefully picked every 500 m. Amplitudes were calibrated against the seabed and its multiples. Hydrophone array directivity and geometrical spreading corrections were also applied. Stacked data were migrated in the time domain using a Stolt algorithm. Depth conversion was carried out with a velocity model obtained by iterative pre-stack depth migration. Red and blue stripes represent positive and negative reflections caused by temperature and salinity variations. Labeled boxes are used for spectral analysis in Figure 3. (b) Spatial distribution of diapycnal diffusivity, $\log_{10} K_t^T$ (m^2 s^{-1}), calculated by fitting vertical displacement spectra with a Batchelor model over the bandwidth 0.015–0.04 cpm. Gray shading = regions with no trackable reflections.

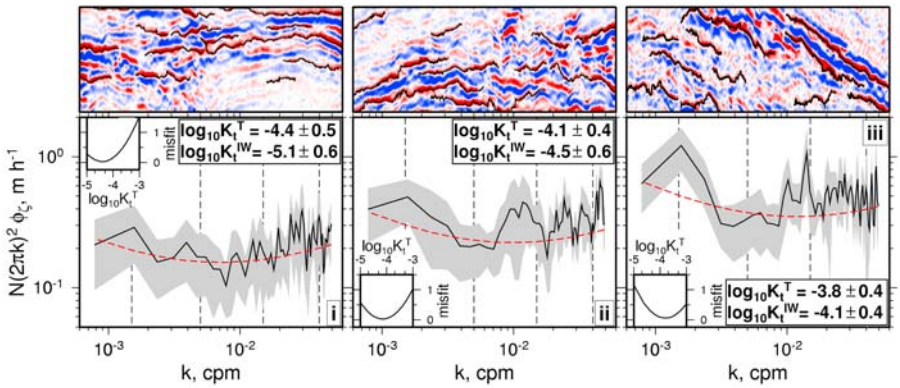

Figure 3. Spectral analyses of 3 boxes shown in Figure 2a. Box dimensions = 12 km × 200 m. (bottom) Normalized spectral density plotted as a function of horizontal wavenumber. Spectral densities have been multiplied by $(2\pi k)^2$ to distinguish internal wave and turbulent regimes (negative and positive slopes, respectively). Solid black line with gray bar = average spectrum calculated from typically 5–20 tracked seismic reflections, with 90% confidence band; dashed red line = best-fit theoretical spectrum calculated from combined internal wave and turbulence model; dashed vertical black lines = bandwidths over which observed and theoretical spectra are matched. Right inset: calculated diapycnal diffusivities (in m^2s^{-1}) and their uncertainties (K_t^{IW} and K_t^T are estimates based upon low wavenumber internal wave regime and high wavenumber turbulent regime, respectively). Left inset: misfit plotted as a function of $\log_{10} K_t$. (top) Portion of seismic data used to compute average spectrum. Red and blue stripes = seismic reflections; black lines = tracked horizons, which were initially identified on a 100 m × 2 m grid. Suitable horizons were then sampled every 10 m.

an exponent of −5/3). *Klymak and Moum* [2007b] show that turbulence and internal wave energy displacement spectra should be summed so that

$$\phi_\zeta = \phi_\zeta^{IW} + \phi_\zeta^T \tag{1}$$

The subscripts *IW* and *T* refer to internal wave and turbulent regimes, respectively. As wave field energy increases, the transition between internal wave and turbulent regimes migrates to lower wavenumbers.

[7] If the wavefield varies slowly with time, the rate of energy transfer from large to small spatial scales equals the rate at which energy is dissipated. The rate of turbulent dissipation measured in W kg^{-1}, ε, can be calculated from the turbulent regime using a simplified version of the *Batchelor* [1959] model:

$$\phi_\zeta^T = \frac{4\pi\Gamma}{N^2} C_T \varepsilon^{2/3} (2\pi k)^{-5/3} \tag{2}$$

where $C_T \approx 0.4$ is a constant term and $\Gamma \approx 0.2$ is the empirically defined mixing efficiency. k is the horizontal wavenumber in cycles per meter (cpm). In the internal wave regime, mixing rates are estimated using the Gregg-Henyey parameterization, which is accurate to within a factor of two [*Gregg*, 1989],

$$\langle \varepsilon \rangle = 7 \times 10^{-10} \frac{N^2}{N_0^2} \left\langle \frac{\phi_\zeta^{IW}}{\phi_\zeta^{GM}} \right\rangle^2 \tag{3}$$

where N is the buoyancy frequency, N_0 = 3 cycles per hour (h^{-1}) is the reference buoyancy frequency and 7×10^{-10} W kg^{-1} is the dissipation of the background GM75 spectrum, ϕ_ζ^{GM}, at 30° latitude. $\langle \ldots \rangle$ denotes the average calculated over the wavenumber bandwidth. The diapycnal diffusivity in m^2 s^{-1}, K_t, is computed for each regime using $K_t = 0.2\varepsilon/N^2$ [*Osborn*, 1980].

[8] Vertical displacements of temperature gradient surfaces are manifest by sub-horizontal seismic reflections. We assume that these surfaces are a reasonable proxy for true isopycnal displacements [*Krahmann et al.*, 2008]. In order to analyze the spatial variation of vertical displacements, the seismic transect was gridded into 12 km × 200 m boxes, which overlap by half their width and depth. Box size was dictated by the requirement to be large enough for a sufficient number of reflections for spectral analysis, without compromising the linearity of displaced surfaces and the homogeneity of wave field energy within a given box. An automated tracking algorithm was used to identify and follow amplitude peaks and troughs within each box [*Holbrook and Fer*, 2005]. Horizons shorter than 1280 m were discarded and tracking was terminated if reflection amplitude dropped below a given noise threshold. Cycle skipping was avoided by limiting the vertical step between picks to 6 m. Tracks which coincide for more than 300 m were omitted. Vertical displacements of a picked horizon were calculated by first subtracting a best-fit straight line from the horizon. Power spectral density estimates of vertical perturbations about this line were calculated using ensemble averaging with a 128 sample wide Hanning window which had no overlap. Individual spectra were averaged over each analysis box.

[9] Internal wave displacements depend upon the local stratification (i.e., N). To correct for this dependence, power spectral densities were normalized by multiplying by an average buoyancy frequency depth profile, which was computed from 7 regional conductivity-temperature-depth casts selected from the British Oceanographic Data Centre dataset (www.bodc.ac.uk). A 20% variation in N produces an error of ± 0.1 in $\log_{10} K_t$.

[10] Three examples of seismic analysis boxes with tracked horizons and corresponding energy spectra are shown in Figure 3. Internal wave and turbulent regimes

are clearly visible in these spectra. Average, best-fit, log-log slopes for the low wavenumber (0.0015–0.005 cpm) and high wavenumber (0.015–0.04 cpm) sub-ranges are -2.5 ± 0.5 and -1.9 ± 0.4, respectively. These values correspond well to the -2.5 and $-5/3$ slopes predicted by the GM75 and turbulent models. Internal wave and turbulent bandwidths were chosen to exclude a transition region within which neither internal waves or turbulence dominate. We have also excluded very low wavenumbers where spectra are band-limited. Very high wavenumbers are probably contaminated by ambient noise. A change in slope typically occurs at 10^{-2}cpm, which corroborates the results of *Klymak and Moum* [2007b] and *Riley and Lindborg* [2008].

[11] To find a best-fitting spectral model for both turbulent and internal wave regimes, we have minimized a trial function

$$M = \sum_{\log_{10} k_1}^{\log_{10} k_2} \left[\log_{10}\left(\phi_\zeta^o(k)/\phi_\zeta^c(k)\right)\right]^2 \Delta(\log_{10} k) \qquad (4)$$

where ϕ_ζ^o and ϕ_ζ^c are the observed and calculated vertical displacement spectra, respectively. Equation (4) is designed to ensure that different wavenumbers are equally weighted in log-log space.

[12] For the turbulent regime, $\phi_\zeta^c = \phi_\zeta^T \equiv A^T k^{-5/3}$, $k_1 = 0.015$ cpm, and $k_2 = 0.04$ cpm; for the internal wave regime, $\phi_\zeta^c = \phi_\zeta^{IW} \equiv A^{IW} k^{-2.5}$, $k_1 = 0.0015$ cpm, and $k_2 = 0.005$ cpm. To start with, each regime is fitted separately by varying A^T or A^{IW}. Then, minimization is carried out across both regimes with $k_1 = 0.0015$ cpm, $k_2 = 0.04$ cpm by varying a composite spectra (equation (1)). A two stage minimization is used since we initially do not know what contribution each regime makes to the fitted bandwidth. Calculated and observed spectra are in good agreement (Figure 3). The misfit function usually has a strong global minimum and a small residual misfit (Figure 3).

[13] Calculated diffusivities range from 10^{-5} to $10^{-3.5}$ m^2 s^{-1}. Values estimated from the internal wave bandwidth using equation (3) predict diffusivities with a mean of $10^{-4.6\pm0.7}$ m^2 s^{-1}. In comparison, the turbulent regime yields estimates which have a mean of $10^{-4.2\pm0.4}$m^2 s^{-1} (equation (2)). *Klymak and Moum* [2007a] suggest that internal wave amplitudes have a weaker dependence on wave energy and cannot easily be used to deduce mixing rates from horizontal measurements alone. Mixing rates are more reliably measured for the turbulent regime [*Klymak and Moum*, 2007b]. Diapycnal diffusivity values computed from the turbulent regime are probably more robust and their spatial distribution is shown in Figure 2b. Mixing rates increase along rougher regions of the seabed and around the side and base of the main lens structure.

4. Discussions and Conclusions

[14] Our results suggest that seismic reflection displacement spectra extracted from acoustic seismic images exhibit a continuum of behavior, which ranges from internal wave type characteristics at lower wavenumbers to more turbulent dominated motions at higher wavenumbers. Observed spectra are red and accurately match a linear combination of GM75 and Batchelor spectral models. The excellent fit between observation and theory enables the spatial variability of diapycnal diffusivities to be estimated within one half of an order of magnitude.

[15] We have analyzed a seismic transect located across the Falkland Plateau in the South Atlantic Ocean, which crosses two lens-shaped homogeneous bodies of water. Inferred diffusivities using the higher wavenumber, turbulent regime, are typically $10^{-4.2\pm0.5}$ m^2 s^{-1}, encouragingly similar to estimates from hydrographic measurements made across the Falkland Plateau by *Naveira Garabato et al.* [2004]. The spatial distribution of mixing is patchy and bears a close relationship to the geometries of acoustically imaged thermohaline features. Smoother, continuous reflections along the top of the lenses are coincident with lower energy levels while increased mixing activity is seen in more disrupted seismic patches located along rougher regions of the seabed and along the sides of the larger lens. The relationship between fine-scale and mesoscale structures provides a useful insight into the spatial pattern of ocean mixing and into the way in which energy cascades between different spatial scales.

[16] Techniques for measuring the spatial distribution of mixing rates from acoustically imaged fine-structure will help to bridge the gap between detailed physical oceanographic measurements and the need to map mixing rates throughout the ocean.

[17] **Acknowledgments.** KLS is supported by the Natural Environment Research Council (NERC) UK and by Schlumberger Cambridge Research. RHW was funded as a NERC Advanced Research Fellow. We are grateful to D. Klaeschen who helped KLS to process seismic data at IFM-GEOMAR and to J. Klymak who generously provided a MATLAB toolbox for computing Garrett-Munk spectra. We also thank C. Caulfield, P. Christie, A. Crosby, P. Haynes, K. Heywood, S. Holbrook, R. Jones, J. Klymak, A. Naveira Garabato, N. Plummer, A. Thompson, C. Trowell, S. Thorpe and A. Woods for their help. Department of Earth Sciences contribution ESC./1119.

References

Arhan, M., A. C. Naveira Garabato, K. J. Heywood, and D. P. Stevens (2002a), The Antarctic Circumpolar Current between the Falkland Islands and south Georgia, *J. Phys. Oceanogr.*, *32*, 1914–1931.

Arhan, M., X. Carton, A. Piola, and W. Zenk (2002b), Deep lenses of circumpolar water in the Argentine Basin, *J. Geophys. Res.*, *107*(C1), 3007, doi:10.1029/2001JC000963.

Batchelor, G. K. (1959), Small-scale variation of convective quantities like temperature in turbulent fluid, *J. Fluid. Mech.*, *5*, 113–139.

Garrett, C., and W. Munk (1975), Space-time scales of internal waves: A progress report, *J. Geophys. Res.*, *80*, 291–297.

Gregg, M. C. (1989), Scaling turbulent dissipation in the thermocline, *J. Geophys. Res.*, *94*, 9686–9698.

Heywood, K. J., A. C. Naveira Garabato, and D. P. Stevens (2002), High mixing rates in the abyssal Southern Ocean, *Nature*, *415*, 1011–1014.

Holbrook, W. S., and I. Fer (2005), Ocean internal wave spectra inferred from seismic reflection transects, *Geophys. Res. Lett.*, *32*, L15604, doi:10.1029/2005GL023733.

Holbrook, W. S., P. Paramo, S. Pearse, and R. W. Schmitt (2003), Thermohaline finestructure in an oceanographic front from seismic reflection profiling, *Science*, *301*, 821–824.

Krahmann, G., P. Brandt, D. Klaeschen, and T. Reston (2008), Mid-depth internal wave energy off the Iberian Peninsula estimated from seismic reflection data, *J. Geophys. Res.*, *113*, C12016, doi:10.1029/2007JC004678.

Klymak, J. M., and J. N. Moum (2007a), Oceanic isopycnal slope spectra. Part I: Internal waves, *J. Phys. Oceanogr.*, *37*, 1215–1231.

Klymak, J. M., and J. N. Moum (2007b), Oceanic isopycnal slope spectra. Part II: Turbulence, *J. Phys. Oceanogr.*, *37*, 1232–1245.

Naveira Garabato, A. C., K. L. Polzin, B. A. Heywood, and K. J. Visbeck (2004), Widespread intense turbulent mixing in the Southern Ocean, *Science*, *303*, 210–213.

Osborn, T. R. (1980), Estimates of the local rate of vertical diffusion from dissipation measurements, *J. Phys. Oceanogr.*, *10*, 83–89.

Riley, J. J., and E. Lindborg (2008), Straitified turbulence: A possible interpretation of some geophysical turbulence measurements, *J. Atmos. Sci.*, *65*, 2416–2424.

Ruddick, B., H. Song, C. Dong, and L. Pinheiro (2009), Water column seismic images as maps of temperature gradient, *Oceanography*, *22*, 192–205.

R. W. Hobbs, Department of Earth Sciences, University of Durham, South Road, Durham DH1 3LE, UK.

K. L. Sheen and N. J. White, Bullard Laboratories, Department of Earth Sciences, University of Cambridge, Madingley Road, Cambridge CB3 OEZ, UK. (kls47@cam.ac.uk)